X-ray Powder Structure Determination and Thermal Behavior of a New Modification of Pb(II) Selenite

Manu Lahtinen* and Jussi Valkonen

The Laboratory of Inorganic and Analytical Chemistry, Department of Chemistry, University of Jyväskylä, P.O. Box 35, FIN 40351, Jyväskylä, Finland

Received November 5, 2001. Revised Manuscript Received January 30, 2002

The crystal structure of a new polymorphic form of lead(II) selenite ($PbSeO_3$) was solved directly from conventional X-ray powder diffraction data. Direct methods and Rietveld refinement techniques were used for the structure determination. The compound crystallizes in the monoclinic space group $P2_1/c$ (no. 14) with cell dimensions $a = 9.1587(1)$ Å, $b = 8.0902(1)$ Å, $c = 8.7932(1)$ Å, $\beta = 103.032(1)°$, and $V = 634.76(2)$ Å^3. The final refinement gave background excluded $R_p = 6.22\%$, $R_{wp} = 8.81\%$, and $R_B = 2.16\%$ by using 45 structural and 15 profile parameters with 10 atoms in an asymmetric unit. The three-dimensional structure consists of 9-coordinated lead atoms, which are linked by three bidentate and three monodentate selenite groups. By combining thermal studies and X-ray powder diffraction, the starting of irreversible phase transition between both polymorphic forms was observed, as now reported structure transformed slowly from space group $P2_1/c$ to the known structural form $P2_1/m$ between 315 and 355 °C.

1. Introduction

The structural information on a compound is essential to understand its physical, chemical, and biochemical properties. A large number of compounds of pigments, pharmaceuticals, catalysts, conductors, ceramics, and polymeric materials can only be synthesized or have been intentionally synthesized as polycrystalline powders. The intense development on powder diffraction based structure determination methods nowadays enables obtaining the structural information on the polycrystalline materials, as the effectiveness of the methodology has been shown for example on zeolites, fullerenes, superconductors, and nanocrystalline solids.[1]

The selenite anion has turned out to be a diverse ligand as depending on reaction conditions, a wide range of basic metal and more complex multication and/or multianion selenites can be prepared. These crystalline solids may contain single or multiple numbers of selenite (SeO_3^{2-}), hydrogen selenite ($HSeO_3^-$), or diselenite ($Se_2O_5^{2-}$) type anions.[2] As presented by the extensive review by Verma, all the alkali and earth alkali metal, most of the p-block, and many of the transition-metal selenites are known.[3] In the case of lead, structural information on various single and more complex compounds of lead selenites are known, such as $PbSeO_3$,[4] $PbSe_2O_5$,[5] $Pb(HSeO_3)_2$,[6] $PbCu_2(SeO_3)_3$[7] and $Pb_2(NO_2)(NO_3)(SeO_3)$.[8] The coordination geometry of Pb^{2+} is intriguing because the stereochemical effects of the lone-pair electrons occasionally cause either apparent caps or other distortions in the coordination chemistry.[9] Furthermore, novel polymorphic forms, metastable materials with unexpected structures and unusual physical properties, may appear as the formation of various selenite compounds are highly dependent on the reaction conditions being used in synthesis.

The synthesis of $PbSeO_3$ is well-known, as it can be prepared via precipitation reaction by straightforward mixing of lead acetate and selenium oxide water solutions at room temperature. However, the crystal structure of resulting product has remained unknown up to the present because the product is only polycrystalline instead of measurable single crystals. The present study deals with the structure determination of polycrystalline $PbSeO_3$ directly from powder diffraction data. Furthermore, the phase transition from space group $P2_1/c$ to the structural form $P2_1/m$ reported by Koskenlinna et al.[4] was observed by combining thermal studies and X-ray powder diffraction. In addition, conventional thermogravimetric (TG) and differential scanning calorimetric (DSC) studies were carried out.

2. Experimental Section

The precipitate of $PbSeO_3$ was obtained by allowing equal quantities (0.9 mol/L) of aqueous solutions of SeO_2 and $Pb(CH_3COO)_2$ to react. White very fine-grained powder formed immediately along with mixing of the reactants. The precipitate was filtered off, washed with deionized water, and dried at room temperature. The molecular formula and the crystal structure were characterized using thermogravimetry and X-ray powder diffraction, respectively. The previously reported form of $PbSeO_3$ was also synthesized. The details for the synthesis are presented elsewhere.[4]

* To whom correspondence should be sent: e-mail makrla@cc.jyu.fi; Tel +358 14 260 2624; Fax +358 14 260 2501.

(1) Louër, D. *Acta Crystallogr.* **1998**, *A54*, 922.
(2) Morris, R. E.; Cheetham, A. K. *Chem. Mater.* **1994**, *6*, 67.
(3) Verma, V. P. *Thermochim. Acta* **1999**, *327*, 63.
(4) Koskenlinna, M.; Valkonen, J. *Cryst. Struct. Commun.* **1977**, *6*, 813.
(5) Koskenlinna, M. *Acta Crystallogr.* **1995**, *C51*, 1.
(6) Koskenlinna, M. *Acta Crystallogr.* **1995**, *C51*, 1737.
(7) Effenberger, H. *J. Solid State Chem.* **1988**, *73*, 118.
(8) Effenberger, H. *Monatsh. Chem.* **1987**, *118*, 211.
(9) Lawton, S. L.; Kokotailo, G. T. *Inorg. Chem.* **1972**, *11*, 363.

10.1021/cm0112690 CCC: $22.00
Published on Web 03/28/2002

The high-resolution X-ray powder diffraction data were obtained at room temperature with a PC-controlled Huber G670 imaging-plate Guinier camera.[10] The sealed-tube X-ray generator system was operated at 45 kV and 25 mA, and pure line-focused Cu Kα_1 radiation ($\lambda = 1.5406$ Å) was produced by a primary beam curved germanium monochromator ($d = 3.266$ Å). The measurement was carried out in Guinier-type transmission geometry with the angle of incidence 45° to the sample normal. The hand-ground samples were prepared on the vaseline-coated Mylar foil of 3.5 μm thickness. The vertical sample holder oscillated horizontally with amplitude of 10 mm to improve the statistics of the measurements. The diffracted X-ray photons with the angular range of 4−100° (2θ) were captured to the curved imaging plate located inside the aluminum detector housing.

After an acquisition time of 60 min the image foil was scanned by a red diode laser to release the diffraction signals in form of diffusely scattered blue photostimulated light, which was concurrently collected by the photomultiplier tube. The whole angular range was scanned six times with step resolution of 0.005 (2θ), thus producing the powder data of 19 200 points. The instrumental resolution of the equipment was determined using highly crystalline silicon standard (SRM 640b, National Institute of Standards & Technology). For silicon, the sharpest full width at half-maximum (fwhm) value of 0.09° (2θ) was obtained from diffraction peak on the 28.44° (2θ). The equipment was aligned and calibrated using a mixture of LaB_6 (SRM 660, National Institute of Standards & Technology) and silicon standards so that an absolute error of less than 0.02° (2θ) on peak positions was achieved.

The extraction of the peak positions for indexing was performed with both the BEDE ZDS SEARCH-MATCH[11] (version 4.21) and GUFI POWDER DIFFRACTION MEASUREMENT AND EVALUATION[12] (version 5.01) software. Both programs were used to verify potential effects for different approaches in determination of peak positions. Before the extraction of the peak positions, the powder diffraction data were gently smoothed and background subtracted by the above programs.

Diffraction pattern indexing was carried out by means of the program CRYSFIRE[13] (version 9.34). The CHEKCELL[14] (17.05.2001) program was used for the space group determination, the program EXPO[15] (version 2000) was used for structure solution, and Rietveld refinements were performed with RIETICA[16] (version 1.71). The software DIAMOND[17] (version 2.1e) was used for structure drawings.

Thermogravimetric studies for both polymorphic forms of $PbSeO_3$ were carried out using a Perkin-Elmer TG7 thermobalance. TG runs were carried out both under synthetic air and nitrogen atmospheres (flow rates of 50 mL/min) from 25 to 850 °C using a heat rate of 2 °C/min. The phase transition study was carried out at room temperature using the described diffraction equipment on the ex situ technique. A larger sample patch (about 1 g) was heated in programmable annealing furnace from RT to 600 °C using heat rate of 6 °C/min. The patch was held at each desired temperature for 30 min before heating to the next observation temperature. A small amount of a sample was extracted out of the patch at selected temperatures following with cooling for 20 min in a desiccator. Powder diffraction data with an acquisition time of 15 min was measured for each sample. The DSC measurements were carried out using a Perkin-Elmer Pyris 1 DSC to confirm the phase transition. The sample was heated first from RT to 375 °C under synthetic air using a heat rate of 6 °C/min followed with cooling back to RT within 20 min, to simulate the procedures carried out with samples extracted from the furnace prior to X-ray diffraction measurements.

Table 1. Crystallographic Data and Parameters of Rietveld Refinement for α-$PbSeO_3$

data collection 2θ range, step resolution (deg)	4−100, 0.005
2θ range used in structure determination (deg)	8.7−83
radiation, λ (Å)	Cu Kα_1, 1.5406
crystal symmetry	monoclinic
space group, Z	$P2_1/c$, 8
formula weight (g/mol)	334.148
color	white
a (Å)	9.1587(1)
b (Å)	8.0902(1)
c (Å)	8.7932(1)
β (deg)	103.032(1)
V (Å^3)	634.76(2)
no. of data points	14 860
no. of reflections	419
profile function	pseudo-Voigt[a]
no. structural parameters	45
no. of constraints	5
no. profile parameters	15
no. of atoms	10
background excluded R_p[b]	6.22%
R_{wp}[b]	8.81%
R_B[b]	2.16%
R_{exp}[b]	3.83%

[a] Asymmetric pseudo-Voigt function (modified Rietveld-type as described on RIETICA), $A_{ihkl} = 1 - AS[\mathrm{sign}(2\theta_i - 2\theta_{hkl})](2\theta_i - 2\theta_{hkl})^2 \cot(\theta_{hkl})$, AS = asymmetry parameter. [b] $R_p = \sum|y_{io} - y_{ic}|/\sum y_{io}$, $R_{wp} = [\sum w_i(y_{io} - y_{ic})^2/\sum w_i y_{io}^2]^{1/2}$, $w_i = 1/(y_{io} + y_{ib})$, $R_B = \sum|I_{hklo} - I_{hklc}|/\sum I_{hklo}$, $R_{exp} = [(N_{obs} - N_{var})/\sum w_i y_{io}^2]^{1/2}$.

3. Structure Determination

All the subprograms included in CRYSFIRE were used for indexing. The number of diffraction lines indexed on the programs was limited to a recommended maximum based on the information given by the corresponding authors. The congruent monoclinic solution were achieved by means of DICVOL,[18] LZON,[19] FJZN,[20] and TREOR[21] with very high figures of merits, such as $M_{20} = 113$ $F_{20} = 193$ (0.0025, 41) on DICVOL. The final unit cell parameters for the structure solution are given in the Table 1. As suggested by the space group analysis of the powder data, the $P2_1/c$ symmetry was successfully used for structure determination. Furthermore, some of the tentative unit cell solutions with lower figures of merits were attempted for structure determination without further success.

The integrated intensities were extracted from the powder data by means of the Le Bail method[22] used in EXPO, following with structure determination by the

(10) Ståhl, K. *J. Appl. Crystallogr.* **2000**, *33*, 394.
(11) Ondrus, P.; Skala, R.; Bowen, K *Bede ZDS Search/Match for Windows*, Prague, Czech Republic, 1999.
(12) Dinnebier, R. *NONIUS-GUFI*, Mineralogisch-Petrographisches Institut, Universität Heidelberg Heidelberg, Germany, 1995.
(13) Shirley, R. *The CRSYFIRE System for Automatic Powder Indexing: User's Manual*; The Lattice Press: England, 1999.
(14) Laugier, J.; Bochu, B *LMGP−Suite: Suite of Programs for the interpretation of X-ray Experiments*, ENSP/Laboratoire des Matériaux et du Génie Physique Saint Martin d'Hères, France, 2000.
(15) Altomare, A.; Burla, M. C.; Camalli, M.; Carrozzini, B.; Cascarano, G.; Giacovazzo, C.; Guagliardi, A.; Moliterni, A. G. G.; Polidori, G.; Rizzi, R. *J. Appl. Crystallogr.* **1999**, *32*, 339.
(16) Hunter, B. A.; Howard, C. J *LHPM-Rietica: a Computer program for Rietveld Analysis of X-ray and Neutron Powder Diffraction Patterns: User's Manual*, Australian Nuclear Science and Technology Organization Lucas Heights Research Laboratories, Menai, Australia, 2000.
(17) Brandenburg, K. *DIAMOND*, Crystal Impact GbR Bonn, Germany, 2000.
(18) Boultif, A.; Louër, D. *J. Appl. Crystallogr.* **1991**, *24*, 987.
(19) Shirley, R.; Louër, D. *Acta Crystallogr.* **1978**, *A34*, 382.
(20) Visser, J. W. *J. Appl. Crystallogr.* **1969**, *2*, 89.
(21) Werner, P.-E.; Eriksson, L.; Westdahl, M. *J. Appl. Crystallogr.* **1985**, *18*, 367.
(22) Le Bail, A.; Duroy, H.; Fourquet, J. L. *Mater. Res. Bull.* **1988**, *23*, 447.

direct methods. The range 8.7−83° (2θ) yielded the best balance between the number of isolated reflections (37%) and overall number of reflections (419) to be used for the structure determination.[23] In a first attempt, two Pb and two Se atom positions were found from the E-maps along with somewhat noncoordinative positions of six oxygen atoms. The positions of oxygen atoms were excluded, and the positional parameters of Pb and Se atoms were used in the second attempt as known fragment to find out the oxygen atoms with better trigonal-pyramidal coordination around Se atoms. As result of the attempt, positional coordinates of six oxygen atoms were found (EXPO: R_p = 6.48%). Additional oxygen atoms were not found despite the fact that Verma et al. suggested a tentative structure of $PbSeO_3 \cdot 2H_2O$ for a compound that was prepared at similar conditions.[24] Finally, the anhydrous crystal structure was confirmed by the thermal studies (see section 4.2). The approximate structure solution was used as starting structural model for final Rietveld refinement using RIETICA.

In the final refinement an asymmetric (Rietveld modified) pseudo-Voigt function was fitted to the line profiles on same angular range than used in the structure determination. The influence of an asymmetry parameter was limited between 8.7 and 40° (2θ) as the asymmetric behavior of peak profiles existed mainly at angles below 40°. Details of the refinement are given in Table 1. The shifted Chebyshev II function consisting of six parameters was used to define the remaining background, as the peak-search programs already subtracted the main part of the background. As transmission geometry with very thin (roughly 0.1 mm) sample thickness was used in the measurements, the absorption effects were expected to be marginal. The order of the refinement followed the general guidelines presented by McCusker et al.[25]

The isotropic thermal parameters were refined with the other structural parameters so that the thermal parameters of heavy atoms were released before releasing of lighter atoms. Thermal parameters of selenium atoms were constrained to vary in same manner. Furthermore, the thermal parameters of the oxygen atoms bonding to the Se1 were constrained to refine equally. The parameters of oxygen atoms bonding to Se2 were treated similarly. Figure 1 shows the final fit from the Rietveld refinement. The final positional coordinates are given in Table 2; selected bond lengths, bond valences, and angles are given in Tables 3 and 4.

4. Results and Discussion

4.1. Description of the Structure. The structure of now reported form of $PbSeO_3$ (hereafter α-$PbSeO_3$) is built from trigonal-pyramidal selenite groups coordinated around the Pb atoms (Figure 2). The asymmetric unit includes two Pb atoms. Both Pb1 and Pb2 atoms are 9-coordinated by oxygen atoms, so that three of the selenite groups are bidentately bonded to each Pb atom. The Pb coordination polyhedra can be described as monocapped square antiprisms, which are highly distorted, compared to the shape of the Pb polyhedra in β-$PbSeO_3$ (Figure 3). One monodentate and three bidentate selenite group oxygen atoms situating on a folded plane form the lower base of the antiprism around Pb1. Two monodentate and two bidentate selenite group oxygen atoms, in which one of the bidentate group oxygen forms the monocap, form the upper base of antiprism. The Pb1−O bond lengths are in the range 2.533−3.039 Å. The mean planes of the polyhedron are almost parallel to each other, but the top base of the polyhedron is "pushed" more to the one side due to the lone-pair effect in the valence shell of the Pb^{2+}.[9] Because

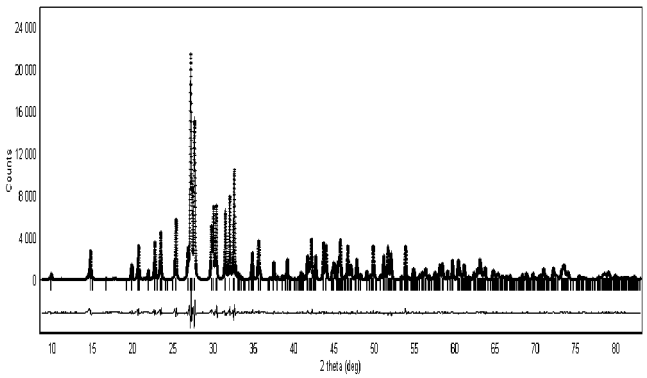

Figure 1. The final Rietveld refinement plot of α-$PbSeO_3$. Observed (marked with +) and calculated (continuous line) lines with difference curve (below tick marks) and tick marks for Bragg line positions.

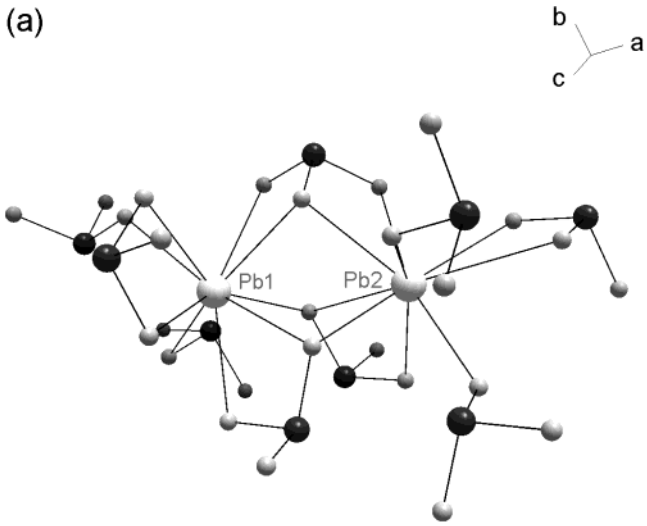

Figure 2. Coordination of neighboring Pb1 and Pb2 atoms for α-$PbSeO_3$, including trigonal-pyramidal selenite groups to show the bidentate and monodentate bonding of selenite groups to the Pb atoms.

Table 2. Final Positional Coordinates and Isotropic Thermal Parameters for α-$PbSeO_3$

atom	*x*	*y*	*z*	occ	B_{iso} (Å^2)
Pb(1)	0.6042(1)	0.1753(1)	−0.273(1)	1	0.79(3)
Pb(2)	0.0045(1)	0.1650(1)	0.1730(1)	1	0.63(3)
Se(1)	0.7953(2)	0.0081(2)	0.4480(3)	1	0.42(3)
Se(2)	0.6810(2)	−0.1006(2)	0.0536(3)	1	0.42(3)
O(1)	0.8673(9)	0.1729(13)	0.3757(10)	1	0.65(16)
O(2)	0.6164(10)	0.0509(11)	0.4040(11)	1	0.65(16)
O(3)	0.8420(10)	0.0500(10)	0.6389(12)	1	0.65(16)
O(4)	0.6641(9)	−0.1477(14)	−0.1423(10)	1	0.88(16)
O(5)	0.6650(10)	0.1106(10)	0.0404(12)	1	0.88(16)
O(6)	0.8647(11)	−0.1211(12)	0.1203(10)	1	0.88(16)

(23) Altomare, A.; Cascarano, G.; Giacovazzo, C.; Guagliardi, A.; Moliterni, A. G. G. *J. Appl. Crystallogr.* **1995**, *28*, 738.
(24) Verma, V. P.; Khushu, A. *J. Therm. Anal.* **1989**, *35*, 1157.
(25) McCusker, L. B.; Von Dreele, R. B.; Cox, D. E.; Louër, D.; Scardi, P. *J. Appl. Crystallogr.* **1999**, *32*, 36.

Table 3. Selected Bond Lengths and Bond Valences for α-$PbSeO_3$[a]

atoms	bond length (Å)	bond valence[b]	atoms	bond length (Å)	bond valence[b]
Pb(1)−O(1)^{i}	2.757(8)	0.17	Pb(2)−O(3)^{vii}	2.586(9)	0.28
Pb(1)−O(2)^{i}	2.695(9)	0.21	Pb(2)−O(4)^{ii}	3.110(9)	0.07
Pb(1)−O(2)^{ii}	2.776(9)	0.17	Pb(2)−O(5)^{v}	3.096(9)	0.07
Pb(1)−O(2)^{iii}	3.039(10)	0.08	Pb(2)−O(6)^{ii}	3.099(10)	0.07
Pb(1)−O(3)^{iii}	2.671(10)	0.22	Pb(2)−O(6)^{viii}	2.598(9)	0.27
Pb(1)−O(4)	2.858(11)	0.13	Pb(2)−O(6)^{v}	2.635(10)	0.24
Pb(1)−O(4)^{iv}	2.796(9)	0.16	Se(1)−O(1)	1.675(10)	1.44
Pb(1)−O(5)^{i}	2.533(10)	0.32	Se(1)−O(2)	1.634(9)	1.61
Pb(1)−O(5)	2.736(10)	0.19	Se(1)−O(3)	1.671(10)	1.46
Pb(2)−O(1)^{v}	2.402(10)	0.46	Se(2)−O(4)	1.737(9)	1.22
Pb(2)−O(1)^{vi}	2.941(9)	0.11	Se(2)−O(5)	1.717(8)	1.29
Pb(2)−O(3)^{vi}	2.724(8)	0.19	Se(2)−O(6)	1.66(1)	1.50

[a] (i) x, 0.5 − y, −0.5 + z; (ii) 1 − x, −y, −z; (iii) x, y, −1 + z; (iv) 1 − x, 0.5 + y, −0.5 − z; (v) −1 + x, y, z; (vi) −1 + x, 0.5 − y, −0.5 + z; (vii) 1 − x, −y, 1 − z; (viii) 1 − x, 0.5 + y, 0.5 − z. [b] $\exp|(r_o - r_{ij})/0.37|$; r_{ij} = bond distance in the structure and r_o = empirically derived cation−anion single bond distance (Pb−O = 2.112 Å, Se−O = 1.811 Å).[30]

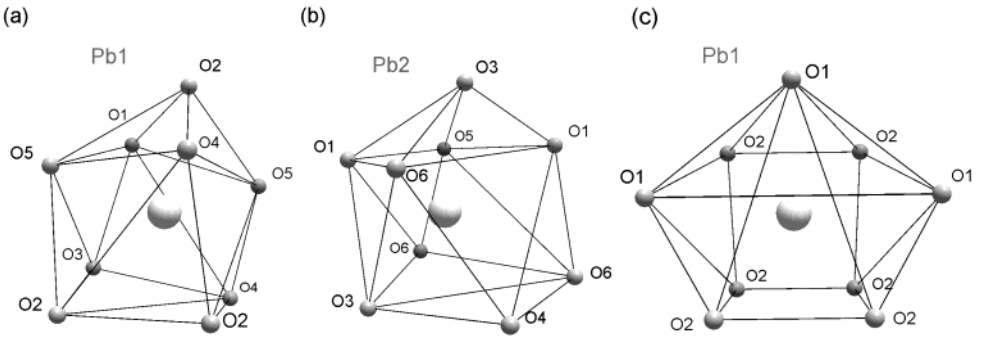

Figure 3. Coordination polyhedra of (a) Pb1, (b) Pb2 atoms of α-$PbSeO_3$, and (c) Pb1 of β-$PbSeO_3$.

Table 4. Selected Bond Angles for α-$PbSeO_3$[a]

atoms	bond angle (deg)	atoms	bond angle (deg)
O(1)−Se(1)−O(2)	101.60(44)	O(2)^{ii}−Pb(1)−O(2)^{i}	135.47(27)
O(1)−Se(1)−O(3)	100.74(44)	O(4)^{iv}−Pb(1)−O(5)	109.47(27)
O(2)−Se(1)−O(3)	102.17(48)	O(2)^{i}−Pb(1)−O(4)	122.69(29)
O(4)−Se(2)−O(5)	99.45(50)	O(3)^{vi}−Pb(2)−O(4)^{ii}	123.24(26)
O(4)−Se(2)−O(6)	100.66(43)	O(6)^{viii}−Pb(2)−O(1)^{vi}	111.22(26)
O(5)−Se(2)−O(6)	100.81(47)	O(3)^{vi}−Pb(2)−O(6)^{ii}	108.03(27)

[a] Symmetry codes have been presented below Table 3.

of that, the difference between the shortest and longest Pb−O distances in the coordination polyhedra varies generally between 0.5 and 1.2 Å in these types of compounds.[5] The closer packing of oxygen atoms in the upper base of the coordination polyhedron is clearly seen as larger bond angles from 109° to 135° for O4−Pb1−O5, O2−Pb1−O2, and O2−Pb1−O4 were observed. Similar widening of the bond angles was observed also in the β-$PbSeO_3$, angles being varied between 107° and 130°.

For Pb2, the coordination polyhedron is formed from monodentate and bidentate selenite groups in a similar manner as on Pb1. The Pb2−O bonds are in the range 2.402−3.110 Å. The bases of the polyhedron are less distorted as compared to Pb1 polyhedron (Table 4). The distance of the Pb1 atom to the plane capped by O2 is shorter (1.06 Å) than to the lower plane (1.88 Å). Similar values were observed both for Pb2 and for Pb atom in the β-form (1.28, 1.69; 0.85, 1.79 Å, respectively). The Se−O bonds are in the range 1.660−1.737 Å, which are similar to distances existing in various metal selenite structures.[2,5,26−28] The polyhedra of both structures are closely packed as all of the selenite oxygen atoms participate in the bonding with Pb atoms. The polyhedron of the β-structure is similarly formed, although it is more ordered due to the mirror plane symmetry. The bond valence sums for the Pb atoms are somewhat less than the common assignment +2 due to fact that the r_0 value (Pb = 2.112 Å) reported by Brown et al.[30] is somewhat shorter than normally appearing in various Pb complexes. For a similar reason the bond valence sums for the Se atoms are somewhat larger than the expected value of +4.

Figure 4a shows the projection of the α-structure along the *c*-axis. The rest of the cell (z = 0.65−1), including four Pb atoms and nine following selenite groups, are omitted for clarity. Two parallel chains of alternating Pb1 and Pb2 atoms occur along the *a*-axis. Because of the complex three-dimensional network structure, similar chains occur also along *b*- and *c*-axes, although along the *c*-axis the chains contain only either Pb1 or Pb2 atoms. A similar network structure occurs also in the β-structure (Figure 4b). The oxygen bonding between the lead atoms is arranged so that two oxygen atoms from separate selenite groups are bonding with the neighboring lead atoms. However, along the *a*-axis, every third connection between Pb1 and Pb2 atoms is formed only via a single selenite group. A similar kind of layout occurs in the β-structure, with exception that the bonding via a single selenite group occurs along the *b*-axis. The lone-pair effect causes the three-dimensional channels to occur throughout the structure in both

(26) Johnston, M. G.; Harrison, W. T. A. *Acta Crystallogr.* **2001**, *E57*, 24.
(27) Valkonen, J. *Acta Crystallogr.* **1994**, *C50*, 991.
(28) Koskenlinna, M. *Acta Crystallogr.* **1995**, *C51*, 1040.
(29) Gospodinov, G. G.; Bogdanov, B. G. *Thermochim. Acta* **1989**, *146*, 15.
(30) Brown, I. D.; Altermatt, D. *Acta Crystallogr.* **1985**, *B41*, 244.

Table 5. Consecutive Stages of the Thermal Decomposition of α-$PbSeO_3$ under Flowing Air

stage	transformation	$\Delta m/m_0$ (%) obsd	$\Delta m/m_0$ (%) calcd	temp range (°C)
1	α-$PbSeO_3 \rightarrow \beta$-$PbSeO_3$			315−355
2	5β-$PbSeO_3 \rightarrow Pb_3O_2(SeO_3) + 2PbSeO_3 + 2SeO_2\uparrow$	14.1	13.3	470−610
3	$Pb_3O_2(SeO_3) + 2PbSeO_3 \rightarrow Pb_5O_4(SeO_3) + 2SeO_2\uparrow$	25.3	26.6	610−720
4	$Pb_5O_4(SeO_3) \rightarrow 5PbO + SeO_2\uparrow$	33.0	33.2	720−780

structures. In the case of the α-structure, the channels are more twisted due to the screw axis and the glide plane symmetry. In the β-structure, selenite groups are arranged in two parallel rows along the *b*-axis. A similar kind of selenite group layer occurs for a second time at $y + 0.5$, $z - 1$. For the α-structure the selenite layers are arranged somewhat differently, as the selenite groups of the two layers reside more in a crosswise formation. The pairs for inverted selenite groups are always located in the parallel row on the same layer, and selenite groups on the second layer are arranged so that in every second group the pyramidal tops of the second layer groups are against the tops of the first layer groups, instead of the oxygen atom cornered bases.

4.2. Thermal Studies. Thermogravimetric studies were carried out to confirm that the compound did not contained water and to compare the thermal decomposition of the both structures. Decomposition paths being presented in the literature are partly contradictory, as various types of dissociation routes are suggested.[24,29]

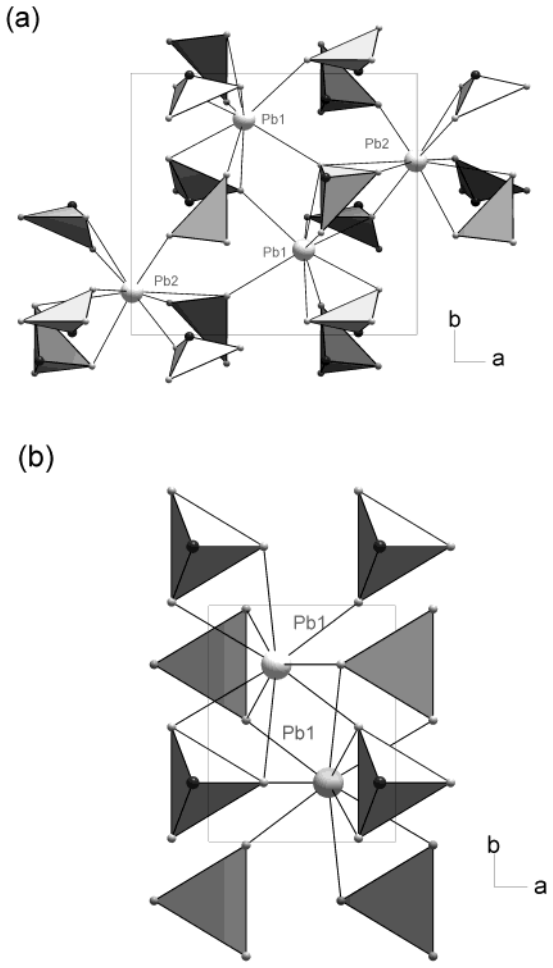

Figure 4. Projection of the structures of (a) α-$PbSeO_3$ (half of the cell omitted along *c*-axis, for clarity; *z*: 0.65−1), and (b) β-$PbSeO_3$ along the *c*-axes. Large light gray circle, Pb; dark gray circle, Se; small light gray circle, O.

In Figure 5 two similarly behaving TG curves are displayed. The light gray curve was recorded from the β-type under nitrogen and the darker one from the α-type recorded under air. The measurements for the both structure types in contrary atmospheric conditions are left out of the figure for clarity, since they were closely analogous to displayed curves. By heating α-$PbSeO_3$ under air (black curve in Figure 5) from room temperature to 470 °C, only minimal (less than 1%) weight loss was observed, indicating potential existing of small amounts of impurities, such as selenium acid and/or moisture (Table 5). However, the α-$PbSeO_3$ transforms slowly to the β-$PbSeO_3$ between 315 and 355 °C as characteristic diffraction peaks for both phases are seen on X-ray data (Figure 6). Based on the DSC studies, the transformation is kinetically very slow and occurs most probably via amorphous phase, as the crystallization peak observed on DSC was weak prolonging to a broad temperature range (Figure 5). Based on the X-ray diffraction studies, the transformation process was finished at 375 °C as only the β-type structure was observed on diffraction data. However, it should be reminded that samples were cooled to RT before the measurements, giving the sample more time to complete the phase transformation. The quickening of the transformation was determined on DSC data as clearer crystallization peak clusters were observed within the cooling stage between 375 and 315 °C. Therefore, it is not fully confirmed that the sample was completely transformed to the β-phase before starting of the second stage in the thermogravimetric studies.

In the second stage the β-phase dissolves between 470 and 610 °C, transforming eventually to mixture of basic β-$PbSeO_3$ and 2PbO·$PbSeO_3$ [$Pb_3O_2(SeO_3)$] as suggested by Gospodinov et al.[29] The mixture of both phases is clearly seen at diffraction data that were measured from the sample being extracted at 600 °C. The theoretical weight loss ($\Delta m/m_0$ 13.3%) is analogous to the observed one (14.1%). Presumably, in the third stage the oxyselenite and rest of the basic lead selenite transforms to

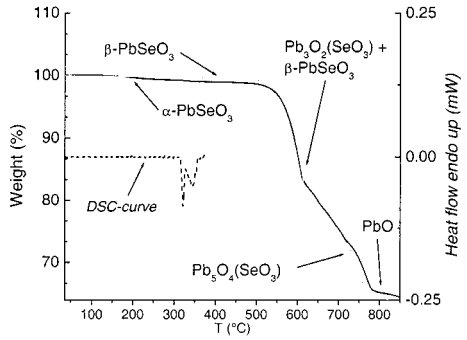

Figure 5. DSC and TG curves of the decomposition of α-$PbSeO_3$ and β-$PbSeO_3$ under flowing air (for α-type) and nitrogen (for β-type) 50 mL/min using heating rate of 2 °C/min from RT to 850 °C. The DSC curve was measured under flowing air 50 mL/min using heating rate of 6 °C/min from 35 to 375 °C.

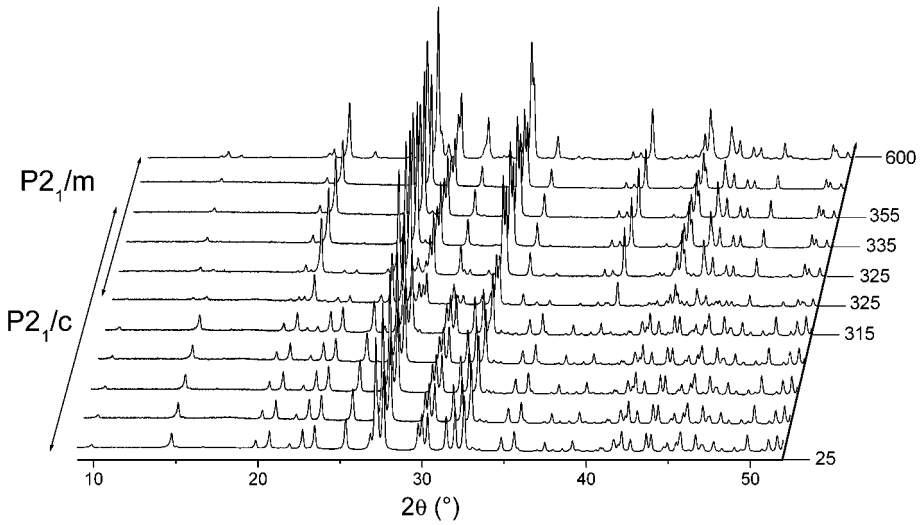

Figure 6. Consecutive diffraction data obtained from the treated samples of α-$PbSeO_3$, which have been extracted from desired temperatures between RT and 600 °C.

$4PbO{\cdot}PbSeO_3$ [$Pb_5O_4(SeO_3)$] with loss of SeO_2 (25.3%), which then in the fourth stage dissociates to the final residue PbO (33.0%). Similar behavior was observed for pure β-$PbSeO_3$ under air atmosphere. In the case of heating under a nitrogen atmosphere (light gray curve) the thermal dissociation of both structure types followed a similar path than observed under air. However, slightly deeper weight loss was observed in the second stage, which was probably caused by somewhat greater loss of SeO_2 if compared to the amount of remaining β-$PbSeO_3$ and oxyselenite phases.

Acknowledgment. We thank Docent Ilkka Pitkänen for helpful discussions concerning the interpretation of the DSC data.

CM0112690